Probing superconducting order in overdoped $Ca_xY_{1-x}Ba_2Cu_3O_7$ by neutron diffraction measurements of the vortex lattice

A. S. Cameron,[1,2,*,†] E. Campillo,[3,4,*,‡] A. Alshemi,[3] M. Bartkowiak,[5] L. Shen,[3] H. Kawano-Furukawa,[6,7] A. T. Holmes,[1,8] O. Prokhnenko,[5] A. Gazizulina,[9] J. S. White,[10] R. Cubitt,[11] N.-J. Steinke,[11] C. D. Dewhurst,[11] A. Erb,[12] E. M. Forgan,[1] and E. Blackburn[1,3]

[1]*School of Physics and Astronomy, University of Birmingham, Edgbaston, Birmingham, B15 2TT, United Kingdom*
[2]*Institut für Festkörper- und Materialphysik, Technische Universität Dresden, D-01069 Dresden, Germany*
[3]*Division of Synchrotron Radiation Research, Lund University, SE-22100 Lund, Sweden*
[4]*Département de Physique, Institut Quantique and Regroupement Québécois sur les Matériaux de Pointe, Université de Sherbrooke, Sherbrooke, J1K 2R1 Quebec, Canada*
[5]*Helmholtz-Zentrum Berlin für Materialien und Energie, Hahn-Meitner-Platz 1, D-14109 Berlin, Germany*
[6]*RIKEN Center for Emergent Matter Science (CEMS), Wako, Saitama 351-0198, Japan*
[7]*Department of Physics, Advanced Sciences, G.S.H.S. Ochanomizu University, Tokyo 112-8610, Japan*
[8]*European Spallation Source ERIC, P.O. Box 176, SE-221 00, Lund, Sweden*
[9]*Karlsruhe Institute of Technology, Institute for Quantum Materials and Technologies, 76021 Karlsruhe, Germany*
[10]*Laboratory for Neutron Scattering and Imaging (LNS), Paul Scherrer Institute (PSI), CH-5232 Villigen, Switzerland*
[11]*Institut Laue Langevin, 71 Avenue des Martyrs, F-38000 Grenoble Cedex 9, France*
[12]*Walther Meissner Institut, BAdW, D-85748 Garching, Germany*

(Received 1 June 2022; revised 15 August 2023; accepted 28 August 2023; published 30 October 2023)

We present small-angle neutron scattering studies of the magnetic vortex lattice (VL) in $Ca_{0.04}Y_{0.96}Ba_2Cu_3O_7$ up to a field of 16.7 T and $Ca_{0.15}Y_{0.85}Ba_2Cu_3O_7$ up to 25 T to investigate the general behavior of the superconducting gap in YBCO-based compounds at high magnetic field. We find in these overdoped compounds that the series of VL structure transitions have shifted down in field relative to those reported for the undoped compound. The hole doping by calcium is expected to alter the Fermi velocity and it reduces the upper critical field of the system. However, we attribute the VL changes mainly to the weakening of the 1D superconductivity in the Cu-O chains by the disorder introduced by doping. The high-field structure of the VL is similar to recent measurements on the parent compound in even higher fields of 25 T, which indicates that the fundamental d-wave nature of the superconducting gap is unchanged by calcium doping. This is corroborated by the temperature dependence of the VL form factor, which also shows the same d-wave behavior as observed in other cuprates. We also argue that they might be the explanation of Pauli paramagnetic effects in the field dependence of the VL form factor.

DOI: 10.1103/PhysRevB.108.144511

I. INTRODUCTION

We report on small angle neutron scattering (SANS) studies of the magnetic vortex lattice (VL) in $Ca_xY_{1-x}Ba_2Cu_3O_7$ (Ca-YBCO), with $x = 0.04$ and 0.15. The parent compound of Ca-YBCO is $YBa_2Cu_3O_7$ ($YBCO_7$), the fully oxygen doped member of the $YBa_2Cu_3O_{7-\delta}$ (YBCO) family. YBCO was the first high T_c superconductor where the mixed state was studied by SANS [1], and since then, VL studies using SANS have continued to provide a wealth of information about its superconducting state [1–16].

Our main interest in this paper is to change the doping of YBCO-based materials to establish the general behavior of the superconducting gap under high fields. Typically, hole doping in YBCO is performed by varying oxygen content on the Cu-O chains. The fully oxygenated compound with $\delta = 0$ is very slightly overdoped but has low pinning due to the absence of oxygen vacancies. To increase the hole concentration further, the system can be doped with calcium, which has one less electron in its outer orbital structure than yttrium. Hole doping in this manner, unlike oxygen doping, does not modify the structure of the copper oxide chains, allowing us to maintain fully occupied chains, while altering hole doping in the planes. However, the Ca dopants may cause extra vortex pinning or tend to disrupt the 1D chain superconductivity. The hole contribution of the Cu-O chains is not trivially related to the oxygen content, being strongly affected by disorder in the chains [17]. Using a phenomenological relation between the critical temperature in YBCO and the hole doping p

*These authors contributed equally to this work.
†alistair.cameron@tu-dresden.de
‡emma.campillo@sljus.lu.se

Published by the American Physical Society under the terms of the Creative Commons Attribution 4.0 International license. Further distribution of this work must maintain attribution to the author(s) and the published article's title, journal citation, and DOI. Funded by Bibsam.

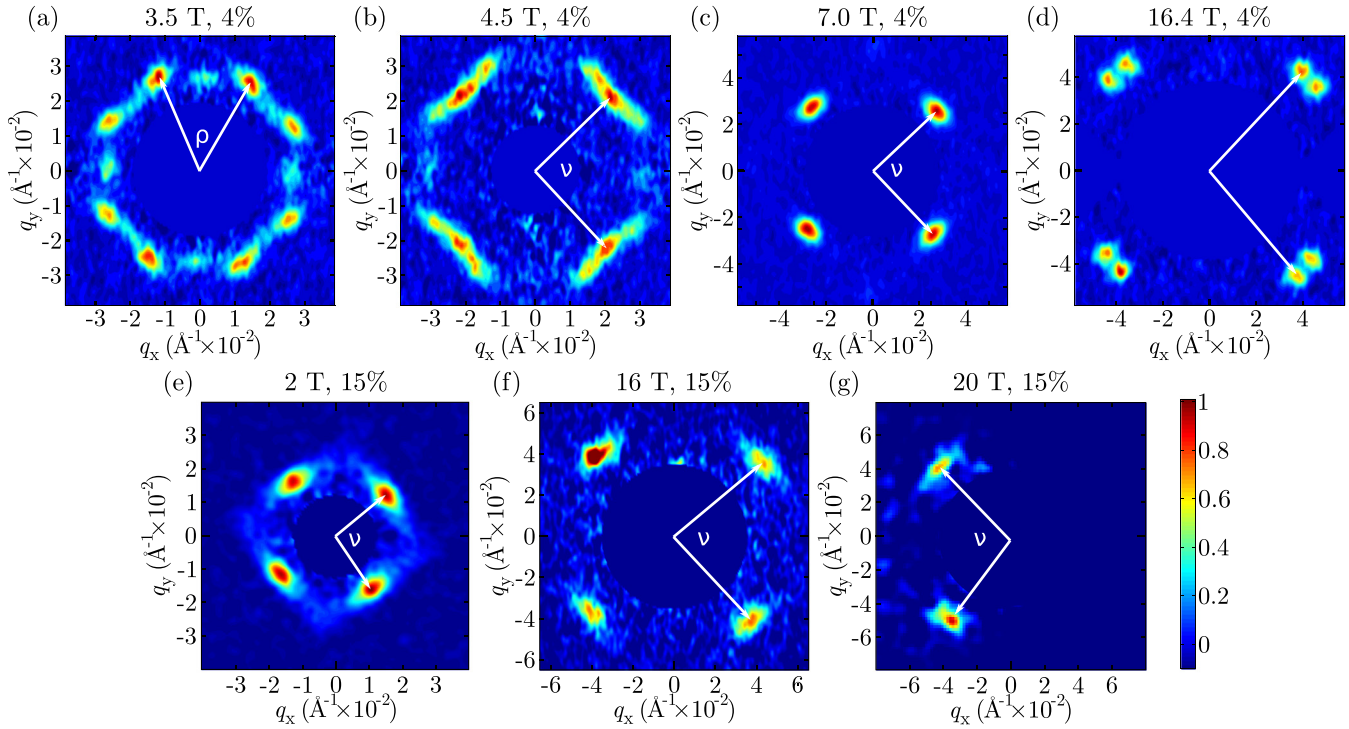

FIG. 1. Diffraction patterns from both the 4% calcium doped sample (a)–(d) and the 15% calcium doped sample (e)–(g), in applied fields of (a) 3 T, (b) 4.5 T, (c) 7 T, (d) 16.4 T, (e) 2 T, (f) 16 T, and (g) 20 T. In (e) and (f), the sample was slightly rotated around the ***c*** axis as compared to the other panels, so the spots are not exactly centered on 45° to the horizontal axis. In (g), measurements were done only for the Bragg condition on the $-q_x$ side. The opening angle of the VL is defined as ρ for the hexagonal lattice and ν for the rhombic lattice, and diffraction patterns are plotted on a normalized intensity scale.

[18], we can estimate that the sample with $x = 0.04$ (T_c = 79 K [19]) has $p = 0.20$, while the $x = 0.15$ sample (T_c = 57 K [19]) has $p = 0.23$. It is also suspected that the chains themselves become superconducting through the proximity effect, potentially adding an *s*-wave admixture to the order parameter of the system [20]. Furthermore, the contribution to the superconducting order parameter from the Cu-O chains behaves differently in YBCO to that in the double-chained $YBa_2Cu_4O_8$ system [12–15,21]. Doping is expected to influence the order parameter in the cuprates [22,23], and doing so with calcium while keeping the chains fully oxygenated provides the opportunity to investigate this without directly introducing disorder in the Cu-O chains. Since the VL is sensitive to the structure of the superconducting order parameter, it is an excellent probe to investigate these matters.

II. EXPERIMENTAL DETAILS

The samples were a mosaic of 12 lightly twinned single crystals of Ca-YBCO with 4% calcium doping, which had been oxygenated to O_7 under high pressure so the Cu-O chains were complete, and a mosaic of three more-heavily twinned single crystals of Ca-YBCO with 15% calcium doping, which had similarly been oxygenated to O_7. Pictures of the samples, characterization of them by magnetization measurements, and polarized-light microscopy are included in the Appendix. The crystals were mounted on plates of high-purity aluminum, coaligned so the **a** and **b** axes were horizontal or vertical and the **c** axis of the crystals were perpendicular to the sample plate. Measurements were taken with the **c** axis of the crystals at 10° to the applied field to reduce the pinning of the flux lines to twin planes [9]. This value of angle was chosen to noticeably reduce vortex pinning, while the effect of the tilted field on the superconducting properties experienced by the VL was small (the superconducting properties are expected to vary as the cosine of the angle between the **c** axis and applied magnetic field [24]). These measurements were performed on the D33 instrument [25] at the Institut Laue-Langevin (ILL) in Grenoble, France [26,27], using the Birmingham 17 T cryomagnet [28], the SANS-I instrument at the Paul Scherrer Institut (PSI) Villigen, Switzerland, using the 11 T cryomagnet, and at the HFM/EXED beamline at HZB, Berlin [29–31].

The data from ILL and PSI were collected in monochromatic mode. The VL was prepared using the oscillation-field-cool method, whereby a small oscillation, on the order of 1%, was made in the magnitude of the applied field as the sample was cooling to base temperature. The resulting data were analyzed using the GRASP analysis package [32] and the diffraction patterns, such as those in Figs. 1(a)–1(f), were treated with a Bayesian method for analysis [33]. After cooling, the field was held fixed during the measurements, and for the scans as a function of temperature, data were taken on warming. Measurements were performed by rotating the sample and applied field together through the Bragg conditions for the VL diffraction spots, with background measurements taken above T_c and subtracted from the low-temperature data to leave only the signal from the VL.

For measurements performed on the HFM/EXED instrument, we relied on the small ripple from the hybrid magnet to provide the oscillation during cooling in field, rather than direct control. This instrument operated using the time-of-flight technique [15,16], which requires one or two fixed magnet rotation angles for the foreground and similarly for the background. These data were analyzed using the MANTID [16,34] software package.

III. RESULTS AND DISCUSSION

A. Field dependence of the vortex lattice structure

Typical VL diffraction patterns from both 4% and 15% doped samples are presented in Fig. 1, illustrating the various VL structures observed as a function of field. From the 4% doped sample, in Fig. 1(a) at 3.5 T we see 12 spots, corresponding to two distorted hexagonal VLs which form in the two domains of the twinned crystals. By comparison with the data from $YBCO_7$ at 5 T, presented in Ref. [13], we can identify the present VL structure with that seen between 2.5 and 6.5 T in the parent compound, which showed weak diffraction spots along the **b*** axis and four stronger off-axis spots. Hence the VL spots bound by the angle ρ in Fig. 1(a) correspond to the crystal domain with **b*** horizontal, along which direction are the two weaker spots from this VL. For a regular hexagonal VL, the diffraction spots lie on a circle, while for a distorted VL they lie on an ellipse, with the amount of distortion characterized by the axial ratio. As in $YBCO_7$, the distortion is consistent with a larger superfluid density along the **b** axis, giving anisotropy in the London penetration depth, arising from superconductivity of the carriers in the chains [13]. We find that the anisotropy is more strongly suppressed by field than in $YBCO_7$ [13] and is nearly absent by 4 T (see inset in Fig. 2). At 4.5 T [Fig. 1(b)], the VL appears somewhat disordered, and mixed phase. We believe this indicates that the VL structure undergoes a first-order transition from the low-field hexagonal lattice [Fig. 1(a)] to a high field rhombic lattice at 4.5 T [Figs. 1(b)–1(d)]. Again, by comparison with the results of Ref. [13], we can identify this with the rhombic structure which appears at 6.5 T and above in $YBCO_7$. In our twinned sample, we would expect two domains to be present. If so, the spots are too close to be clearly resolved when the phase first appears. Alternatively, in this field region, the VL structure may be pinned to the twin planes, which would give spots at 45° to the crystal axes. At first glance, it appears that between 4.5 T and 8 T there is a square phase, shown in Fig. 1(c), which then undergoes a transition to the rhombic phase, which is clearly present in Fig. 1(d). However, upon closer inspection, it is seen that the VL diffraction spots in the "square" phase elongate tangentially with increasing field before separating. This indicates that the higher field region is a single rhombic phase, with a lattice close to square at fields just above the transition, and continuous evolution of its structure with field causing the diffraction spots from the two different domains to separate at higher fields. In the 15% doped sample, in Figs 1(e)–1(g), it appears that only the rhombic high-field phase is present.

The VL structures as expressed by the opening angles ρ and ν, defined in Fig. 1, are shown in Fig. 2. For the 4% sample, the low field hexagonal phase is slightly distorted, with an opening angle ρ of less than 60°. The first-order transition to the rhombic phase is seen at 4.5 T, after which the lattice structure evolves smoothly with increasing field until around 13 T. From here we see that the structure remains constant to the highest applied field of 16.7 T, with an opening angle ν of around 100°. From comparison of the field dependence of ν with that seen in the undoped compound, we expect that the rhombic spots labeled by ν in Fig. 1(d) arise from the VL in the crystal domains that have **b*** horizontal, and the spots closer to the horizontal arise from the VL in the crystal domains that have **b*** vertical. A low-field hexagonal to a high-field rhombic VL transition is characteristic of the cuprates, and is taken to be an indication of the predominantly d-wave order parameter. In comparison with the parent compound, however, we only observe two of the three structure phases found in $YBCO_7$ [12,13], which exhibits two hexagonal (low field and midfield) and one rhombic (high-field) VL structure phases (see Fig. 3). The single hexagonal phase we have observed in 4% Ca-YBCO is analogous to the midfield hexagonal phase of $YBCO_7$. However, we cannot rule out the presence of the low-field phase in 4% Ca-YBCO because the VL diffraction pattern is too disordered below an applied field of 2 T to determine the VL coordination and orientation precisely. Returning to the midfield hexagonal to rhombic transition in 4% Ca-YBCO, this takes place at a lower field than the same transition in $YBCO_7$ and a field-independent value of ν above ∼13 T seen here is not observed within the same field range in the parent compound. Rather, the rhombic phase in $YBCO_7$ appears to be evolving towards a field-independent ν at around 23–25 T [15]. These observations indicate that the

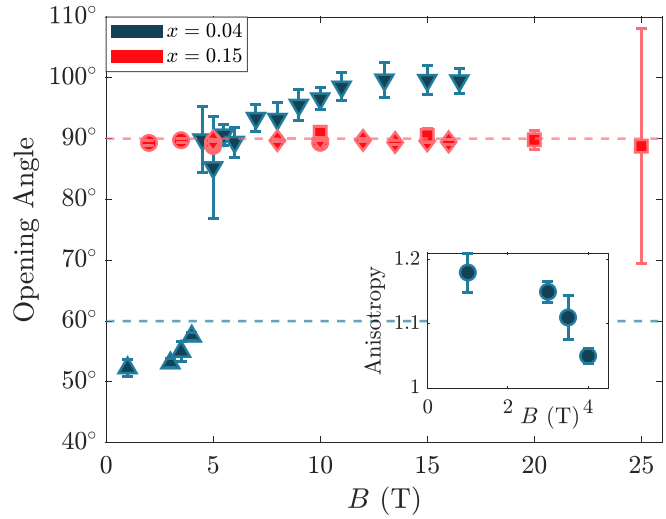

FIG. 2. Opening angle of the VL as a function of applied magnetic field. Dashed lines indicate the opening angle for a hexagonal and square lattice, with the respective angles for the measured VL, ρ and ν, defined in Fig. 1. x refers to the Ca-doping level in $Ca_xY_{1-x}Ba_2Cu_3O_7$. Dark blue △ and ▽ symbols correspond to the data obtained at ILL for $Ca_{0.04}Y_{0.96}Ba_2Cu_3O_7$. The dark blue ○ symbols (inset) correspond to the anisotropy of the VL (defined in the main text). Red points correspond to data from $Ca_{0.15}Y_{0.85}Ba_2Cu_3O_7$; ○ data were obtained at PSI, the ◇ symbols correspond to data measured at ILL, and the red □ symbols are from HFM/EXED.

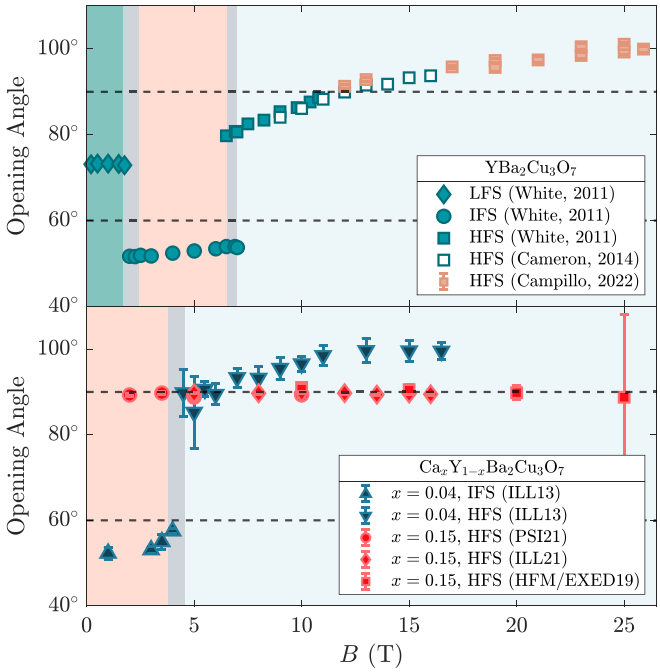

FIG. 3. Opening angle of the VL as a function of applied magnetic field for $YBa_2Cu_3O_7$ and $Ca_xY_{1-x}Ba_2Cu_3O_7$. Dashed lines indicate the opening angle for a hexagonal and square lattice. Meanwhile, $YBa_2Cu_3O_7$ passes through a low field structure (LFS), an intermediate field structure (IFS), and stabilizes in a high field structure (HFS). $Ca_{0.04}Y_{0.96}Ba_2Cu_3O_7$ goes through the IFS and also stabilizes in the HFS, and $Ca_{0.15}Y_{0.85}Ba_2Cu_3O_7$ remains at the HFS for the entire field range.

VL in 4% Ca-YBCO possesses a similar phase diagram to its parent compound, but shifted down in field by approximately a factor of 2. For the 15% sample, the opening angle *appears* in Fig. 2 to remain at 90°, but the spots in Figs. 1(e)–1(g) are elongated tangentially, like those in Fig. 1(c). We take this to indicate that in this sample too, the true value of ν would be $>90°$, but this is obscured by the stronger effects of twin-plane pinning in the 15% Ca-doped sample.

The VL structure transitions observed here, and in other systems, can be attributed to anisotropies in both the electronic structure and the superconducting gap. In general, VL structure theories attempt to model this either by considering an anisotropic Fermi velocity in the presence of an isotropic superconducting gap or vice versa [35–44]. We find several problems when drawing comparisons between these models and our results. First, these theories tend to discuss tetragonal systems, whereas ours is orthorhombic. Consequently, they predict a high-field square VL structure rather than the rhombic lattice we find here. Second, as was noted in work on $YBCO_7$ [12,13], they predict a single 45° rotational transition between two distorted hexagonal phases rather than the 90° transitions observed in the YBCO compounds discussed here. However, beyond this we are able to draw qualitative comparisons between the theory and our results. In both the β model of Suzuki *et al.* [42] and the model of Affleck *et al.* [39], which, respectively, consider anisotropy in Fermi velocity and the superconducting gap, the transition to the high-field structure moves to lower fields as the anisotropy in either the Fermi velocity or the gap is increased. This suggests these anisotropies are more pronounced in Ca-YBCO. There are also first-principles calculations using Eilenberger theory, which have predicted that at high field the vortex nearest-neighbor directions align along the nodes of the order parameter [41]. Our observation that—in the high-field limit of our experiments—the VL nearest-neighbor directions are essentially the same in 4% Ca-YBCO, and $YBCO_7$ indicates that calcium doping leaves the superconducting gap node directions little changed in this region. However, increased hole doping does cause the upper critical field to fall [45], so it seems likely that the addition of calcium is reducing the field scale by this means. We note that there is contradictory evidence in the literature regarding the influence of calcium doping on the hole content of the CuO_2 planes. Raman spectroscopy measurements suggest that Ca atoms form independent nanophases in the material, which would mean that additional carriers from the calcium do not contribute to doping [46], whereas scanning tunneling spectroscopy measurements have indicated that calcium doping does contribute additional holes to the system [22]. Our measurements, showing clear differences in the field scale of VL transitions in $YBCO_7$ and Ca-YBCO, support the latter scenario. However, characteristic fields can be identified for both $YBCO_7$ and Ca-YBCO, in particular, the field at which the opening angle stops changing and the point at which the opening angle goes through 90°. The fields for the 4% doping are approximately a factor of two smaller than in $YBCO_7$. This is larger than expected given the different T_c values and the effect of hole doping on the critical field [45]. Indeed, Grissonnanche *et al.* [45] found that a 5% doped sample has an upper critical field that is two-thirds that of $YBCO_7$, and so we suspect that disorder from the calcium doping may be weakening the 1-D superconductivity in the Cu-O chains. We note that thermal fluctuations in high-T_c materials smear phase transitions in high magnetic fields, so the term "upper critical field" represents the place on a phase diagram near zero temperature where there is a rapid crossover of macroscopic properties.

B. Field dependence of VL form factor

The spatial variation of magnetic field within the VL, expressed by the VL form factor, is shown in Fig. 4 for the diffraction spots seen in Fig. 1. The form factor is a Fourier component of the field variation at the scattering vector $\mathbf{q}$, and is related to the integrated intensity, $I(\mathbf{q})$, as measured by SANS, through the relation [47]

$$I(\mathbf{q}) = 2\pi V \phi \left(\frac{\gamma}{4}\right)^2 \frac{\lambda_n^2}{\Phi_0^2 q} |F(\mathbf{q})|^2. \quad (1)$$

Here V is the sample volume, ϕ is the flux of incident neutrons, γ is the magnetic moment of the neutron in nuclear magnetons (1.91), λ_n is the wavelength of the incident neutrons, and Φ_0 is the flux quantum, $h/2e$. The spatial variation of field within the mixed state is determined both by the London penetration depth λ and the coherence length of the Cooper pairs ξ. For an orthorhombic superconductor with the field applied parallel to the **c** axis of the material, the form factor can be expressed by the anisotropic extended London

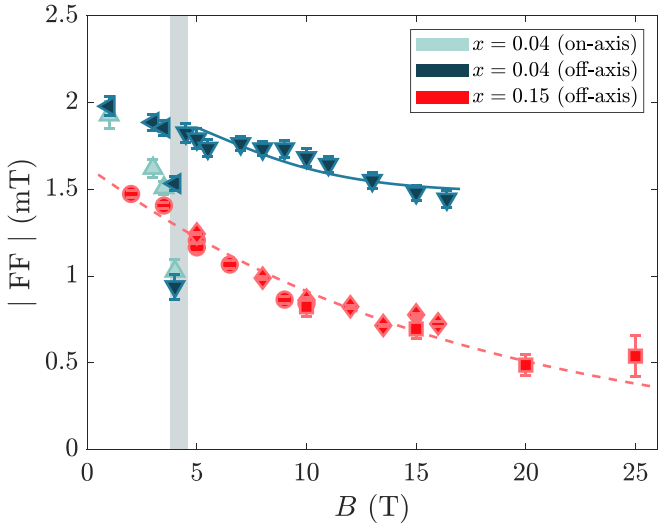

FIG. 4. Vortex lattice form factor as a function of applied magnetic field. x refers to the Ca-doping level in $Ca_xY_{1-x}Ba_2Cu_3O_7$. The shaded grey area defines the phase transition between low- and high-field phases for the 4% sample, which is observed in Fig. 1(b), where both phases are present. The solid line is a fit of the 4% high field data to the model of Eq. (2) and the lower dashed line is a fit to the 15% data using the extended London model. Dark blue △ and ▽ symbols correspond to data obtained at ILL for $Ca_{0.04}Y_{0.96}Ba_2Cu_3O_7$. Red points correspond to data from $Ca_{0.15}Y_{0.85}Ba_2Cu_3O_7$; the ○ data were obtained at ILL, the (◇) symbols correspond to data measured at ILL and the □ symbols are from data obtained at HFM/EXED.

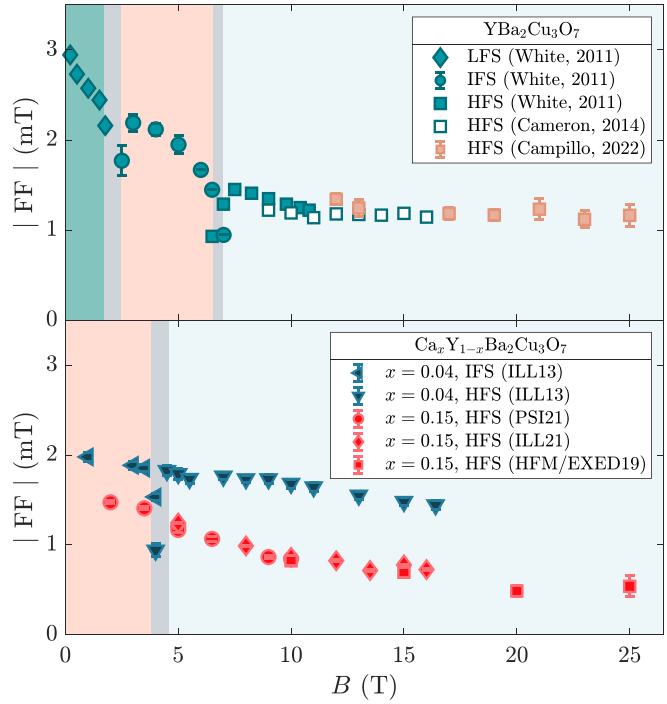

FIG. 5. Form factor of the VL as a function of applied magnetic field for $YBa_2Cu_3O_7$ and $Ca_xY_{1-x}Ba_2Cu_3O_7$.

model [48–50],

$$F(\mathbf{q}) = \frac{\langle B\rangle \exp\left(-c\left(q_x^2\xi_b^2 + q_y^2\xi_a^2\right)\right)}{q_x^2\lambda_a^2 + q_y^2\lambda_b^2}, \tag{2}$$

where $\langle B\rangle$ is the average internal induction, ξ_i is the coherence length along axis i, λ_i is the penetration depth arising from supercurrents flowing in direction i, and q_x, q_y are in-plane Cartesian components of the scattering vector, with q_x parallel to $\mathbf{b}^*$. The parameter c accounts for the finite size of the vortex cores, and a suitable value for c in our field and temperature range is 0.44 [15]. For fields close to B_{c1}, the denominator needs an additional $+1$, but for the fields employed here, this addition is negligible. We can use the basal plane values of the characteristic lengths when the field is applied at 10° to the **c** axis, because their angle-dependence is slower than the cosine of the tilt angle, and $\cos(10^\circ) = 0.985$, which is very close to unity.

We find, however, no values of λ and ξ for which Eq. (2) is able to fit the full range of 4% data in Fig. 4. The fit presented in this figure is for the high-field phase only. We use a modified anisotropic London model as in Ref. [15], with the basal-plane penetration depths linked as follows:

$$\lambda_b^2(B) = \lambda_a^2\{1 + 0.4 \cdot \tanh\left[(B - 5\,\mathrm{T})/7\,\mathrm{T}\right]\}. \tag{3}$$

This equation differs from that used in Ref. [15]; the crossover field of 5 T is half that used for $YBCO_7$.

This fit returns a value for $\lambda_a = 168(3)$ nm. The value for the London penetration depth seems quite reasonable, being slightly higher than for the parent compound $YBCO_7$. The fitted coherence length would be the average of that in the a and b directions (because the Bragg reflections are close to {110} directions), but it is unphysically small (0.14 Å). On the other hand, assuming that the field scale has been suppressed still further, the 15% Ca-doped form factor was fitted with a constant penetration depth to the extended London model, giving reasonable ab-average values of $\lambda = 179(3)$ nm and $\xi = 2.64(8)$ nm [$B_{c2} = 47(3)$ T].

This deviation of the form factor from the extended London model was also observed within previous SANS studies on the parent compound [13–15], although this began at the much higher field of ∼12 T, and continued through to the highest measured field of 25 T (shown in Fig. 5). In the original study where the deviation of the form factor from the model was reported, it was suspected that disorder in the VL was contributing to a static Debye-Waller effect, which reduced scattering from the VL at lower fields [14]. With increasing field, the corresponding increase in the intervortex interaction was proposed to overcome the pinning of the flux lines to defects in the crystal lattice, reducing the static Debye-Waller effect and leading to the apparent increase in the VL form factor which rendered the London model unable to fit the data. Corroborating evidence for this was seen in the temperature dependence of the VL form factor, where indications of an irreversibility temperature suggesting the crossing of a glass-solid transition were seen. However, in the temperature-dependent data presented in Fig. 6, which will be discussed in detail later, we see no indication of such an irreversibility temperature.

We therefore turn to the possibility of the Pauli paramagnetic effect, whereby the Fermi surface splitting of spin-up and spin-down electrons by the Zeeman effect leads to the

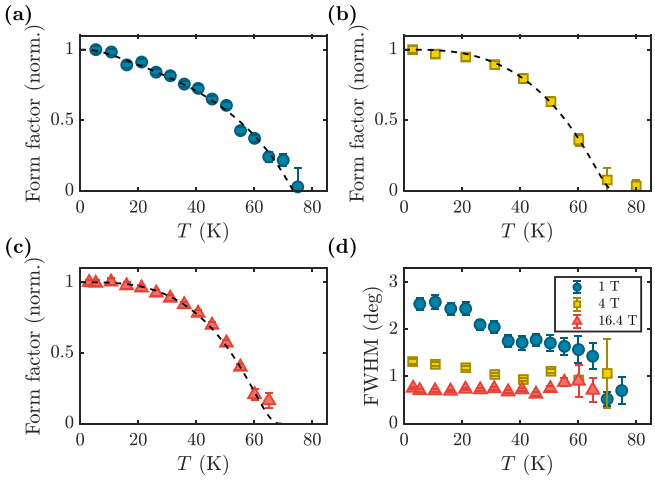

FIG. 6. Vortex lattice form factor as a function of temperature in an applied field of (a) 1 T, (b) 4 T, and (c) 16.4 T. The solid line in (a) is a fit to the anisotropic London model using a d-wave gap described in the text. (d) Variation of the rocking curve FWHM as a function of temperature for the data presented in (a)–(c).

paramagnetic breaking of Cooper pairs. Pauli paramagnetic pair breaking is one of two possible mechanisms by which superconductivity is destroyed at H_{c2}, so at such low fields it is not expected to be relevant in the bulk. However, within the vortex core region, the Cooper pairs are much less strongly bound, and so this can lead to the formation of a paramagnetic moment and the corresponding alteration of the vortex core structure [51,52]. This would increase the field contrast between the cores and the bulk which is observed as a corresponding increase in the VL form factor. This has also been observed in heavy-fermion superconductors [52–54], a borocarbide [55], and an iron-based superconductor [56]. We have speculated that in $YBa_2Cu_3O_7$ the continued deviation of the VL form factor in the parent compound at the highest measured fields [15] could have a similar origin. While the models constructed to describe the behavior of the heavy fermion system, $CeCoIn_5$ [57,58], are not quantitatively appropriate for our results, we can draw several qualitative conclusions from them, and from more recent work [52]. First, since we are at relatively small fractions of H/H_{c2}, we expect the Pauli contribution to be small compared to the orbital component, leading to a deviation from the London model as we see here rather than the dominance of Pauli effects. Second, we expect the effect of Pauli paramagnetism to be larger in Ca-YBCO than the parent compound, since the effect is proportional to the effective mass which has been seen to be increasing with doping in this region of the cuprate phase diagram [59,60]. This correlates with our observation here that the form factor in Ca-YBCO deviates from the London model at fields as low as 5 T, while in the parent compound, it remained London-like until around 12 T, and further supports our earlier conclusion that calcium doping contributes holes to the system.

C. Vortex lattice at higher temperatures

We have measured the temperature dependence of the VL signal in 4% Ca-YBCO. The angle between the VL vectors was found to be temperature independent in these measurements, and the rocking curve width, shown in Fig. 6(d), remains reasonably constant with increasing temperature except at the lowest measured field of 1 T. This is in contrast to $YBCO_7$ at high field, which had a temperature dependence to the VL structure above an identifiable irreversibility temperature, which was visible both as a change in the angle between the VL vectors and the FWHM of the rocking curves [14]. Passing above the irreversibility temperature was seen to reduce the static Debye-Waller factor, leading to a corresponding increase in the integrated intensity of the rocking curves. This rendered the temperature dependence of the VL form factor at high field unsuitable for fitting to models which had proved successful at lower fields and in other superconductors. The absence of both a strong temperature-dependent rocking curve width and an identifiable irreversibility temperature suggests that the VL is strongly pinned by the effects of the Ca dopants. Therefore, we expect that the variation of the VL form factor with temperature, which is shown in Figs. 6(a)–6(c), is not affected by changes in the perfection of the VL, allowing us to investigate the gap structure in this material.

To fit the temperature dependence of the normalized VL form factor, we used Eq. (2) with temperature-dependent penetration depths. λ_a^2 and λ_b^2 are, respectively, inversely proportional to the in-plane components ρ_{aa} and ρ_{bb} of the superfluid density. To obtain the temperature dependence, we followed the method that has been used to model the VL form factor in both cuprate and pnictide superconductors [13–15,61,62],

$$(\rho_{aa}(T),\ \rho_{bb}(T)) = 1 - \frac{1}{2\pi k_B T}\int_0^{2\pi} (\cos^2(\phi),\ \sin^2(\phi)) \times \int_0^{\infty} \cosh^{-2}\left(\frac{\sqrt{\varepsilon^2 + \Delta_{\mathbf{k}}^2(T,\phi)}}{2k_B T}\right) d\phi d\varepsilon, \quad (4)$$

where $\rho_{aa}(T)$ and $\rho_{bb}(T)$ are normalized to their values at temperature $T = 0$, ϕ is the azimuthal angle about the Fermi surface, and $\sqrt{\varepsilon^2 + \Delta_{\mathbf{k}}^2(T,\phi)}$ gives the excitation energy spectrum. The gap function was assumed to be separable into temperature and momentum-dependent factors such that $\Delta_{\mathbf{k}}(T,\phi) = g_{\mathbf{k}}(\phi)\Delta_0(T)$, where $g_{\mathbf{k}}(\phi)$ describes the momentum-dependent gap as a function of angle around the Fermi surface. The temperature dependence of the gap, $\Delta_0(T)$, can be approximated by

$$\Delta_0(T) = \Delta_0(0)\tanh\left(\frac{\pi}{\alpha}\sqrt{a\left(\frac{T_c}{T} - 1\right)}\right), \quad (5)$$

where Δ_0 is the magnitude of the gap at zero temperature and α and a are parameters related to the pairing state [63]. BCS d-wave pairing is represented by $\alpha = 2.14$ and $a = 4/3$. For larger values of the gap expected in high-T_c materials, we retain the BCS temperature dependence of the gap (values of α and a) but expect $\Delta_0(0)$ to be of the order of $3\,T_c$ [64]. For the angle dependence of the gap in the high-field limit, we take [15,63]

$$g_{\mathbf{k}}(\phi) = \cos(2\phi) + \delta, \quad (6)$$

where $\delta = 0.17$ represents the shift of the nodes in the energy gap away from 45° to the crystal axes.

It has been previously noted in the cuprates that nonlocal effects can become increasingly important with field, which leads to a flattening of the temperature dependence of the superfluid density at low temperature. Work by Amin *et al.* [40,43] showed that in the nonlocal regime, below a characteristic temperature T^*, the linear temperature dependence flattens out to a T^3 dependence. This behavior can be represented by the relation [13]

$$n_s(T) = 1 - (1 - n_s(T))\left(\frac{T_c + T^*}{T_c}\right)\left(\frac{T^2}{T^2 + (T^*)^2}\right), \quad (7)$$

where n_s is the superfluid density, as calculated above in the local limit. T^* is field-dependent parameter given by $T^* \sim \Delta_0(\xi_0/d) \propto \sqrt{H}$.

We employed the Ginzburg-Landau relation for the field dependence of the gap, $\Delta(B)/\Delta(0) = (1 - (B/B_{c2})^2)^{1/2}$, and a phenomenological relation for the critical temperature, $T_c(B) = T_c(0)(1 - B/B_{c2})^{1/2}$ [65]. The fits used $B_{c2} = 100$ T, which is a reasonable estimation for the upper critical field [45], and a critical temperature $T_c = 76$ K, which is slightly lower than other reported values, but was consistent with all three sets of data we fitted.

We present the fits of the d-wave model with nonlocal corrections to the temperature dependence of the form factor in Fig. 6(a). Starting with the 1 T data in Fig. 6(a), we expect a T^* of around 6 K from the BCS gap of $2.14\,T_c$, using the value of the critical field to estimate ξ_0. Leaving the magnitude of Δ_0 as the free parameter of the fit, such that T^* is determined by Δ_0, we find that it returns a value of $\Delta_0 = (3.21 \pm 0.09)\,T_c$, which corresponds to a $T^* = 9.7$ K. While this gap value is ∼50 % larger than the weak-coupling BCS value, we note that large gap values in cuprates are not unusual [66], so this is a reasonable value. The fit is clearly a good description of the data, and possesses the finite low-temperature slope characteristic to nodal gap structures, indicating that this material is d wave in nature, and that as expected the nonlocal effects do not contribute strongly at low field.

For the fits at 4 T and 16.4 T, if we follow the Ginzburg-Landau relation for the field dependence of the gap, we would expect the gap value at 4 T to be $3.20\,T_c$ with $T^* \sim 20$ K, and at 16.4 T the gap to be $3.12\,T_c$ with $T^* \sim 40$ K. However, we find that these parameters are not able to fit the data. Indeed, following the predicted $\sqrt{H}$ dependence for T^* does not allow for the fitting of the data for any value of the gap. We have therefore kept the Ginzburg-Landau relation for the gap, which gives the values described above, but left T^* as a variable parameter in these fits. This gives $T^* = 59 \pm 3$ K at 4 T and $T^* = 70 \pm 3$ K at 16.4 T. This is higher than expected, with $T^* \approx T_c$ at the highest measured fields. This suggests that the onset of nonlocal effects is both more rapid and stronger with increasing field than the current models would predict.

IV. CONCLUSIONS

We have investigated the VL structure of calcium-doped YBCO and have compared the behavior of the VL in these overdoped materials with that of pure $YBCO_7$. The results from the 15% doped sample are dominated by pinning to the large density of twin planes, but the 4% doping shows similar behavior to $YBCO_7$, but with a lower field scale. In the limit of high fields, both systems show the same VL structure. Therefore, we conclude that the underlying gap structure is unaffected by the change in doping and is the same in both the calcium-doped systems and the parent compound. We attribute the different field scales in the VL structural transitions mainly to the weakening of the 1D superconductivity in the Cu-O chains by the disorder introduced by doping, although the upper critical field will also be reduced by overdoping. Furthermore, in the 4% Ca-doped sample, the field dependence of the form factor can only be fit to the anisotropic London model with unphysically small coherence lengths. This compares with the reported behavior in $YBCO_7$ where the anisotropic London model cannot be fit at high fields with any reasonable coherence length. We speculate that this is due to the onset of a significant Pauli paramagnetic contribution inside the vortex cores as a function of field.

ACKNOWLEDGMENTS

This paper is based on experiments performed at the Institut Laue-Langevin (ILL), Grenoble, and the Swiss spallation neutron source SINQ, Paul Scherrer Institute, Villigen, Switzerland, and Helmholtz-Zentrum Berlin (HZB). A.S.C., A.T.H., E.M.F., and E.B. gratefully acknowledge support by the UK Engineering and Physical Sciences Research Council (EPSRC) through Grants No. EP/J016977/1 and No. EP/G027161/1. E.M.F. was supported by the Leverhulme Foundation. A.S.C. acknowledges support from the German Research Foundation (DFG) under Grant No. IN 209/3-1. A.A. acknowledges support from the Crafoord Foundation, Dnr. 20190930. We would like to thank R. Wahle, S. Gerischer, S. Kempfer, P. Heller, K. Kiefer, and P. Smeibidl for their support during the HFM/EXED experiment. We thank J. Baglo, M. Mezidi, and S. Fortier, members of the Taillefer group of the Université de Sherbrooke, for assistance and resources for completing sample characterization.

APPENDIX

We include a brief summary of the characterization of the samples used during the neutron scattering measurements. In Figs. 7(a) and 7(b), we show pictures of the mosaic samples used for the neutron experiments mentioned above. To reveal the twinning present in both samples, we have also taken polarized-light pictures of the 4% Ca-doped YBCO sample [Fig. 7(c)] and of the 15% [Fig. 7(d)]. We can observe in both samples the different domains, revealed as dark and light regions, which have crystal a axes along one or another of the directions at 45° to the domain boundaries. It can be clearly observed in the 15% Ca-doped YBCO sample that the widths of the domains are much narrower than in the 4% Ca-doped YBCO sample. Thus, the 15% Ca-doped YBCO sample is more highly twinned and this explains the strong pinning effects present in this sample.

We have also performed several magnetization measurements using a vibrating sample magnetometer from 0 to 16 T

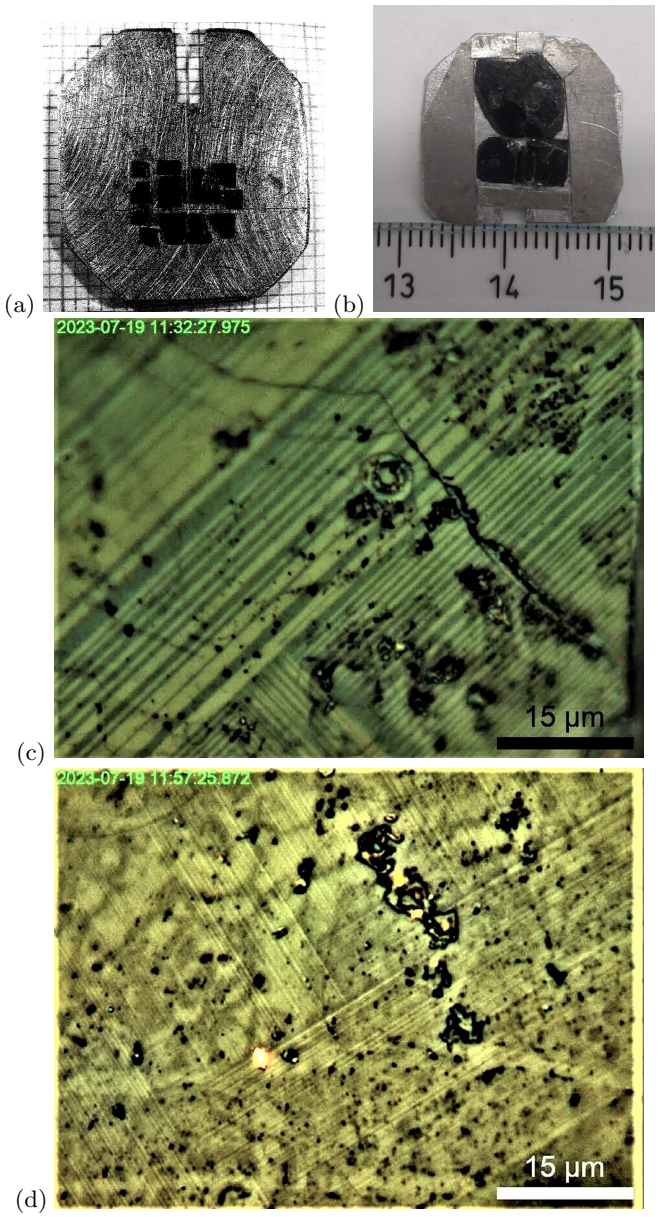

FIG. 7. (a) Photograph of the 4% doped sample. (b) Photograph of the 15% doped sample. Polarized-light pictures of the (c) 4% and (d) 15% Ca-doped YBCO samples where the widths of the domains are not greater than 2.2 and 0.4 μm, respectively.

on both samples. However, during measurements of a hysteresis loop, the 15% Ca-doped YBCO sample broke, limiting

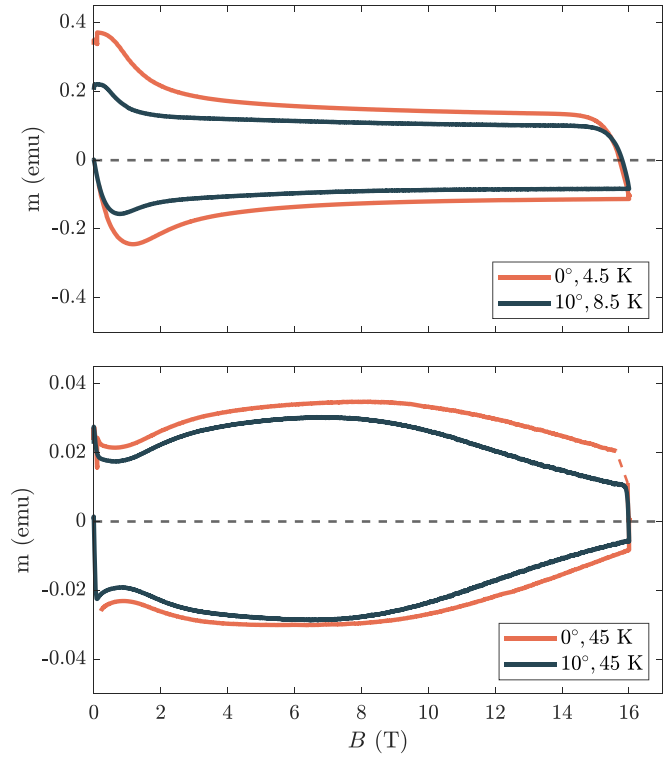

FIG. 8. Magnetization curves of the 4% Ca-doped YBCO sample measured at low temperatures (top) and at $T_c/2$ (bottom) where the critical current is around $J_c \approx 6 \cdot 10^6$ A/m^2. The PPMS was unable to reach lower temperatures than 8 K during the low-temperature measurements at 10°. The dashed line in the bottom panel represents a region where the VSM was not measuring.

measurements on this sample. This was due to the torque created by the VL pinning at high magnetic fields applied at 10° to the **c** axis. In Fig. 8, we show the magnetization curves measured on the 4% Ca-doped YBCO sample measured at low temperatures (4.5 K and 8.5 K) applying the magnetic field parallel to the **c** axis and also tilted 10° as in the neutron scattering experiments (Fig. 8, top). The same magnetization curves were repeated at $\sim T_c/2$ (Fig. 8, bottom). The hysteresis in the magnetization curves reveals the strength of the pinning (corresponding to the critical current density $J_c \gtrsim 10^6$ A/m^2 at 45 K). We see that tilting the field by 10° reduces the pinning by a small fraction, and so conclude that the main cause of the pinning is due to the Ca doping. However, the twin boundaries are still mainly responsible for the flux-lattice orientation in the 15% sample.

[1] E. M. Forgan, D. M. Paul, H. A. Mook, P. A. Timmins, H. Keller, S. Sutton, and J. S. Abell, Observation by neutron diffraction of the magnetic flux lattice in single-crystal $YBa_2Cu_3O_{7-\delta}$, Nature (London) **343**, 735 (1990).

[2] M. Yethiraj, H. A. Mook, G. D. Wignall, R. Cubitt, E. M. Forgan, D. M. Paul, and T. Armstrong, Small-angle neutron scattering study of flux line lattices in twinned $YBa_2Cu_3O_7$, Phys. Rev. Lett. **70**, 857 (1993).

[3] M. Yethiraj, H. A. Mook, G. D. Wignall, R. Cubitt, E. M. Forgan, S. L. Lee, D. M. Paul, and T. Armstrong, Anisotropic vortex lattice in $YBa_2Cu_3O_7$, Phys. Rev. Lett. **71**, 3019 (1993).

[4] B. Keimer, F. Doğan, I. A. Aksay, R. W. Erwin, J. W. Lynn, and M. Sarikaya, Inclined-field structure, morphology, and pinning of the vortex lattice in microtwinned $YBa_2Cu_3O_7$, Science **262**, 83 (1993).

[5] B. Keimer, W. Y. Shih, R. W. Erwin, J. W. Lynn, F. Dogan, and I. A. Aksay, Vortex lattice symmetry and electronic structure in $YBa_2Cu_3O_7$, Phys. Rev. Lett. **73**, 3459 (1994).

[6] E. M. Forgan and S. L. Lee, Comment on "Vortex lattice symmetry and electronic structure in $YBa_2Cu_3O_7$," Phys. Rev. Lett. **75**, 1422 (1995).

[7] C. M. Aegerter, S. T. Johnson, W. J. Nuttall, S. H. Lloyd, M. T. Wylie, M. P. Nutley, E. M. Forgan, R. Cubitt, S. L. Lee, D. McK. Paul, M. Yethiraj, and H. A. Mook, Observation of vortex lattice melting in twinned $YBa_2Cu_3O_{7-x}$ using neutron small-angle scattering, Phys. Rev. B **57**, 14511 (1998).

[8] S. T. Johnson, E. M. Forgan, S. H. Lloyd, C. M. Aegerter, S. L. Lee, R. Cubitt, P. G. Kealey, C. Ager, S. Tajima, A. Rykov, and D. M. Paul, Flux-line lattice structures in untwinned $YBa_2Cu_3O_{7-\delta}$, Phys. Rev. Lett. **82**, 2792 (1999).

[9] S. P. Brown, D. Charalambous, E. C. Jones, E. M. Forgan, P. G. Kealey, A. Erb, and J. Kohlbrecher, Triangular to square flux lattice phase transition in $YBa_2Cu_3O_7$, Phys. Rev. Lett. **92**, 067004 (2004).

[10] C. Simon, A. Pautrat, G. Poullain, C. Goupil, C. Leblond-Harnois, X. Chaud, and A. Brûlet, Influence of twin boundaries on the flux-line-lattice structure in $YBa_2Cu_3O_{7-\delta}$: A small-angle neutron scattering, Phys. Rev. B **70**, 024502 (2004).

[11] J. S. White, S. P. Brown, E. M. Forgan, M. Laver, C. J. Bowell, R. J. Lycett, D. Charalambous, V. Hinkov, A. Erb, and J. Kohlbrecher, Observations of the configuration of the high-field vortex lattice in $YBa_2Cu_3O_7$: Dependence upon temperature and angle of applied field, Phys. Rev. B **78**, 174513 (2008).

[12] J. S. White, V. Hinkov, R. W. Heslop, R. J. Lycett, E. M. Forgan, C. Bowell, S. Strässle, A. B. Abrahamsen, M. Laver, C. D. Dewhurst *et al.*, Fermi surface and order parameter driven vortex lattice structure transitions in twin-free $YBa_2Cu_3O_7$, Phys. Rev. Lett. **102**, 097001 (2009).

[13] J. White, R. Heslop, A. Holmes, E. Forgan, V. Hinkov, N. Egetenmeyer, J. Gavilano, M. Laver, C. Dewhurst, R. Cubitt *et al.*, Magnetic-field-induced nonlocal effects on the vortex interactions in twin-free $YBa_2Cu_3O_7$, Phys. Rev. B **84**, 104519 (2011).

[14] A. S. Cameron, J. S. White, A. T. Holmes, E. Blackburn, E. M. Forgan, R. Riyat, T. Loew, C. D. Dewhurst, and A. Erb, High magnetic field studies of the vortex lattice structure in $YBa_2Cu_3O_7$, Phys. Rev. B **90**, 054502 (2014).

[15] E. Campillo, M. Bartkowiak, R. Riyat, E. Jellyman, A. Cameron, A. Holmes, O. Prokhnenko, W.-D. Stein, A. Erb, E. Forgan *et al.*, Deviations from the extended London model at high magnetic fields in $YBa_2Cu_3O_7$, Phys. Rev. B **105**, 184508 (2022).

[16] E. Campillo, M. Bartkowiak, O. Prokhnenko, P. Smeibidl, E. M. Forgan, and E. Blackburn, Analysis of time-of-flight small-angle neutron scattering data on mesoscopic crystals such as magnetic vortex lattices, J. Appl. Crystallogr. **55**, 1314 (2022).

[17] J. D. Jorgensen, B. W. Veal, A. P. Paulikas, L. J. Nowicki, G. W. Crabtree, H. Claus, and W. K. Kwok, Structural properties of oxygen-deficient $YBa_2Cu_3O_{7-\delta}$, Phys. Rev. B **41**, 1863 (1990).

[18] J. L. Tallon, C. Bernhard, H. Shaked, R. L. Hitterman, and J. D. Jorgensen, Generic superconducting phase behavior in high-T_c cuprates: T_c variation with hole concentration in $YBa_2Cu_3O_{7-\delta}$, Phys. Rev. B **51**, 12911(R) (1995).

[19] C. Bernhard and J. L. Tallon, Thermoelectric power of $Y_{1-x}Ca_xBa_2Cu_3O_{7-\delta}$: Contributions from CuO_2 planes and CuO chains, Phys. Rev. B **54**, 10201 (1996).

[20] J. R. Kirtley, C. C. Tsuei, Ariando, C. J. M. Verwijs, S. Harkema, and H. Hilgenkamp, Angle-resolved phase-sensitive determination of the in-plane gap symmetry in $YBa_2Cu_3O_{7-\delta}$, Nat. Phys. **2**, 190 (2006).

[21] J. S. White, C. J. Bowell, A. S. Cameron, R. W. Heslop, J. Mesot, J. L. Gavilano, S. Strässle, L. Mächler, R. Khasanov, C. D. Dewhurst *et al.*, Magnetic field dependence of the basal-plane superconducting anisotropy in $YBa_2Cu_4O_8$ from small-angle neutron scattering measurements of the vortex lattice, Phys. Rev. B **89**, 024501 (2014).

[22] N.-C. Yeh, C.-T. Chen, G. Hammerl, J. Mannhart, A. Schmehl, C. W. Schneider, R. R. Schulz, S. Tajima, K. Yoshida, D. Garrigus *et al.*, Evidence of doping-dependent pairing symmetry in cuprate superconductors, Phys. Rev. Lett. **87**, 087003 (2001).

[23] G. Deutscher, Coherence and single-particle excitations in the high-temperature superconductors, Nature (London) **397**, 410 (1999).

[24] L. J. Campbell, M. M. Doria, and V. G. Kogan, Vortex lattice structures in uniaxial superconductors, Phys. Rev. B **38**, 2439 (1988).

[25] C. Dewhurst, D33—a third small-angle neutron scattering instrument at the Institut Laue Langevin, Meas. Sci. Technol. **19**, 034007 (2008).

[26] A. Cameron, T. Loew, E. Blackburn, C. Dewhurst, M. Egetenmeyer, E. M. Forgan, V. Hinkov, A. T. Holmes, D. Inosov, B. Keimer, L. Lemberger, J. Lim, J. P. Porras Perez Guerrero, and J. White, Vortex lattice study of highly ordered underdoped $YBa_2Cu_3O_{6+x}$ ($x = 0.5$, 0.7), Institut Laue-Langevin (ILL), doi:10.5291/ILL-DATA.542-347 (2013).

[27] E. Campillo, A. Alshemi, T. Assefa, E. Blackburn, A. Cameron, R. Cubitt, E. M. Forgan, H. Furukawa, A. T. Holmes, and L. Shen, The vortex lattice transition at high fields in $Y_{0.85}Ca_{0.15}Ba_2Cu_3O_7$, Institut Laue-Langevin (ILL), doi:10.5291/ILL-DATA.541-1079 (2021).

[28] A. T. Holmes, G. R. Walsh, E. Blackburn, E. M. Forgan, and M. Savey-Bennett, A 17 T horizontal field cryomagnet with rapid sample change designed for beamline use, Rev. Sci. Instrum. **83**, 023904 (2012).

[29] O. Prokhnenko, W.-D. Stein, H.-J. Bleif, M. Fromme, M. Bartkowiak, and T. Wilpert, Time-of-flight extreme environment diffractometer at the Helmholtz-Zentrum Berlin, Rev. Sci. Instrum. **86**, 033102 (2015).

[30] Helmholtz-Zentrum Berlin für Materialien und Energie, HFM/EXED: The high magnetic field facility for neutron scattering at BER II, JLSRF **3**, A115 (2017).

[31] P. Smeibidl, M. Bird, H. Ehmler, I. Dixon, J. Heinrich, M. Hoffmann, S. Kempfer, S. Bole, J. Toth, O. Prokhnenko, and B. Lake, First hybrid magnet for neutron scattering at Helmholtz-Zentrum Berlin, IEEE Trans. Appl. Supercond. **26**, 4301606 (2016).

[32] C. D. Dewhurst, Graphical reduction and analysis small-angle neutron scattering program GRASP, J. Appl. Cryst. **56**, 1595 (2023).

[33] A. T. Holmes, Simple Bayesian method for improved analysis of quasi-two-dimensional scattering data, Phys. Rev. B **90**, 024514 (2014).

[34] O. Arnold, J. Bilheux, J. Borreguero, A. Buts, S. Campbell, L. Chapon, M. Doucet, N. Draper, R. Ferraz Leal, M. Gigg *et al.*, Mantid-Data analysis and visualization package for neutron scattering and μ SR experiments,

Nucl. Instrum. Methods Phys. Res., Sect. A **764**, 156 (2014).

[35] V. G. Kogan, M. Bullock, B. Harmon, P. Miranović, L. Dobrosavljević-Grujić, P. L. Gammel, and D. J. Bishop, Vortex lattice transitions in borocarbides, Phys. Rev. B **55**, R8693 (1997).

[36] V. G. Kogan, P. Miranović, L. Dobrosavljević-Grujić, W. E. Pickett, and D. K. Christen, Vortex lattices in cubic superconductors, Phys. Rev. Lett. **79**, 741 (1997).

[37] V. Kogan, A. Gurevich, J. Cho, D. Johnston, M. Xu, J. Thompson, and A. Martynovich, Nonlocal electrodynamics and low-temperature magnetization of clean high-κ superconductors, Phys. Rev. B **54**, 12386 (1996).

[38] M. Franz, I. Affleck, and M. H. S. Amin, Theory of equilibrium flux lattices in unconventional superconductors, Phys. Rev. Lett. **79**, 1555 (1997).

[39] I. Affleck, M. Franz, and M. H. S. Amin, Generalized London free energy for high-T_c vortex lattices, Phys. Rev. B **55**, R704(R) (1997).

[40] M. H. S. Amin, I. Affleck, and M. Franz, Low-temperature behavior of the vortex lattice in unconventional superconductors, Phys. Rev. B **58**, 5848 (1998).

[41] M. Ichioka, A. Hasegawa, and K. Machida, Field dependence of the vortex structure in d-wave and s-wave superconductors, Phys. Rev. B **59**, 8902 (1999).

[42] K. M. Suzuki, K. Inoue, P. Miranović, M. Ichioka, and K. Machida, Generic first-order orientation transition of vortex lattices in type II superconductors, J. Phys. Soc. Jpn. **79**, 013702 (2010).

[43] M. H. S. Amin, M. Franz, and I. Affleck, Effective "penetration depth" in the vortex state of a d-wave superconductor, Phys. Rev. Lett. **84**, 5864 (2000).

[44] N. Nakai, P. Miranović, M. Ichioka, and K. Machida, Reentrant vortex lattice transformation in fourfold symmetric superconductors, Phys. Rev. Lett. **89**, 237004 (2002).

[45] G. Grissonnanche, O. Cyr-Choinière, F. Laliberté, S. René de Cotret, A. Juneau-Fecteau, S. Dufour-Beauséjour, M.-E. Delage, D. LeBoeuf, J. Chang, B. Ramshaw *et al.*, Direct measurement of the upper critical field in cuprate superconductors, Nat. Commun. **5**, 3280 (2014).

[46] E. Liarokapis, D. Palles, D. Lampakis, G. Böttger, K. Conder, and E. Kaldis, Phase separation in fully oxygenated $Y_{1-y}Ca_yBa_2Cu_3O_x$ compounds, Phys. Rev. B **71**, 014303 (2005).

[47] D. K. Christen, F. Tasset, S. Spooner, and H. A. Mook, Study of the intermediate mixed state of niobium by small-angle neutron scattering, Phys. Rev. B **15**, 4506 (1977).

[48] J. R. Clem, Simple model for the vortex core in a type II superconductor, J. Low Temp. Phys. **18**, 427 (1975).

[49] Z. Hao and J. R. Clem, Reversible magnetization and torques in anisotropic high-κ type-II superconductors, Phys. Rev. B **43**, 7622 (1991).

[50] A. Yaouanc, P. Dalmas de Réotier, and E. H. Brandt, Effect of the vortex core on the magnetic field in hard superconductors, Phys. Rev. B **55**, 11107 (1997).

[51] M. Ichioka and K. Machida, Vortex states in superconductors with strong Pauli-paramagnetic effect, Phys. Rev. B **76**, 064502 (2007).

[52] E. Campillo, R. Riyat, S. Pollard, P. Jefferies, A. Holmes, R. Cubitt, J. White, J. Gavilano, Z. Huesges, O. Stockert *et al.*, Observations of the effect of strong Pauli paramagnetism on the vortex lattice in superconducting $CeCu_2Si_2$, Phys. Rev. B **104**, 184508 (2021).

[53] A. D. Bianchi, M. Kenzelmann, L. DeBeer-Schmitt, J. S. White, E. M. Forgan, J. Mesot, M. Zolliker, J. Kohlbrecher, R. Movshovich, E. D. Bauer, J. L. Sarrao, Z. Fisk, C. Petrovic, and M. R. Eskildsen, Superconducting vortices in $CeCoIn_5$: Toward the Pauli-limiting field, Science **319**, 177 (2008).

[54] J. S. White, P. Das, M. R. Eskildsen, L. DeBeer-Schmitt, E. M. Forgan, A. D. Bianchi, M. Kenzelmann, M. Zolliker, S. Gerber, J. L. Gavilano, J. Mesot, R. Movshovich, E. D. Bauer, J. L. Sarrao, and C. Petrovic, Observations of Pauli paramagnetic effects on the flux line lattice in $CeCoIn_5$, New J. Phys. **12**, 023026 (2010).

[55] L. DeBeer-Schmitt, M. R. Eskildsen, M. Ichioka,. K. Machida, N. Jenkins, C. D. Dewhurst, A. B. Abrahamsen, S. L. Bud'ko, and P. C. Canfield, Pauli paramagnetic effects on vortices in superconducting $TmNi_2B_2C$, Phys. Rev. Lett. **99**, 167001 (2007).

[56] S. Kuhn, H. Kawano-Furukawa, E. Jellyman, R. Riyat, E. Forgan, M. Ono, K. Kihou, C. Lee, F. Hardy, P. Adelmann *et al.*, Simultaneous evidence for Pauli paramagnetic effects and multiband superconductivity in KFe_2As_2 by small-angle neutron scattering studies of the vortex lattice, Phys. Rev. B **93**, 104527 (2016).

[57] V. Michal and V. Mineev, Paramagnetic effects in vortex lattice field distribution in strongly type-II superconductors, Phys. Rev. B **82**, 104505 (2010).

[58] P. D. de Réotier and A. Yaouanc, Form factor, standard deviation, and skewness of the field distribution in a hard type-II heavy-fermion superconductor from the Ginzburg-Landau model, Phys. Rev. B **84**, 012503 (2011).

[59] B. Ramshaw, S. Sebastian, R. McDonald, J. Day, B. Tan, Z. Zhu, J. Betts, R. Liang, D. Bonn, W. Hardy *et al.*, Quasiparticle mass enhancement approaching optimal doping in a high-T_c superconductor, Science **348**, 317 (2015).

[60] C. Putzke, L. Malone, S. Badoux, B. Vignolle, D. Vignolles, W. Tabis, P. Walmsley, M. Bird, N. E. Hussey, C. Proust *et al.*, Inverse correlation between quasiparticle mass and T_c in a cuprate high-T_c superconductor, Sci. Adv. **2**, e1501657 (2016).

[61] H. Kawano-Furukawa, C. J. Bowell, J. White, R. Heslop, A. Cameron, E. Forgan, K. Kihou, C. Lee, A. Iyo, H. Eisaki *et al.*, Gap in KFe_2As_2 studied by small-angle neutron scattering observations of the magnetic vortex lattice, Phys. Rev. B **84**, 024507 (2011).

[62] R. Morisaki-Ishii, H. Kawano-Furukawa, A. S. Cameron, L. Lemberger, E. Blackburn, A. T. Holmes, E. M. Forgan, L. M. DeBeer-Schmitt, K. Littrell, M. Nakajima *et al.*, Vortex lattice structure in $BaFe_2(As_{0.67}P_{0.33})_2$ via small-angle neutron scattering, Phys. Rev. B **90**, 125116 (2014).

[63] R. Prozorov and R. W. Giannetta, Magnetic penetration depth in unconventional superconductors, Supercond. Sci. Technol. **19**, R41 (2006).

[64] H. Padamsee, J. Neighbor, and C. Shiffman, Quasiparticle phenomenology for thermodynamics of strong-coupling superconductors, J. Low Temp. Phys. **12**, 387 (1973).

[65] M. Tinkham, *Introduction to Superconductivity* (McGraw-Hill, New York, 1996).

[66] M. Hashimoto, I. M. Vishik, R.-H. He, T. P. Devereaux, and Z.-X. Shen, Energy gaps in high-transition-temperature cuprate superconductors, Nat. Phys. **10**, 483 (2014).